Journal of Hazardous Materials 209–210 (2012) 146–150

Contents lists available at SciVerse ScienceDirect

Journal of Hazardous Materials

journal homepage: www.elsevier.com/locate/jhazmat

A new alkali-activated steel slag-based cementitious material for photocatalytic degradation of organic pollutant from waste water

Yao Jun Zhang*, Li Cai Liu, Yong Xu, Ya Chao Wang, De Long Xu

College of Material Science and Engineering, Xi'an University of Architecture and Technology, Xi'an 710055, People's Republic of China

ARTICLE INFO

Article history:
Received 27 November 2011
Received in revised form
11 December 2011
Accepted 1 January 2012
Available online 10 January 2012

Keywords:
Ion exchange
Photocatalysis
Degradation
Steel slag

ABSTRACT

A new type of Ni,Ca-cementitious material was firstly synthesized via a two-step reaction of alkali-activated steel slag polymerization and ion exchange. The XRF results showed that almost all the Na^+ ions in the matrix of Na,Ca-cementitious material were replaced by Ni^{2+} ions at room temperature. The new hydrated products of metahalloysite ($Si_2Al_2O_5(OH)_4$) and calcium silicate hydrate (CSH) were formed in the Na,Ca-cementitious material. The diffuse reflectance UV–vis near infrared ray spectrum was blue-shifted due to the strong interaction between Ni^{2+} and negative charge of $[AlO_4]^{5-}$ tetrahedron in the framework of cementitious material. The Ni,Ca-cementitious material was used as a catalyst for the photocatalytic degradation of methylene blue dye and showed a degradation rate of 94.39% under UV irradiation. The high photocatalytic degradation activity was suggested to be the synergistic effect of the cementitious matrix, Ni^{2+} ions and the iron oxides of wustite (FeO) and calcium iron oxide ($Ca_2Fe_2O_5$) from the steel slag. A probable mechanism of photocatalytic oxidative degradation was proposed.

1. Introduction

Preparation of geopolymers by alkaline activation of the industrial by-products and the natural mine, such as fly ash [1–3], blast furnace slag [4–7], steel slag [8–10] and kaolinite [11,12], have attracted considerable attention due to their excellent physical properties for potential applications in building industry [13,14], encapsulation of radioactive [15], solidification of hazardous wastes [16,17], fire-resistance [18,19] and adsorbents [20–22]. It is suggested that the frameworks of geopolymers consist of $[SiO_4]^{4-}$ and $[AlO_4]^{5-}$ tetrahedra linked randomly by sharing all the oxygen atoms, and the negative charge of $[AlO_4]^{5-}$ tetrahedron is balanced by extra-framework cations of Na^+, K^+ and Ca^{2+} ions [23,24]. In general, the extra-framework cations can be replaced by cations through ion-exchange reaction due to the porous structures of geopolymers [25,26]. Sazama et al. [27] reported that the geopolymer catalysts with Co and Cu cations were prepared by ion exchange reactions of metakaolin-based Na-geopolymer and metakaolin-slag based K,Ca-geopolymer, and were used as the selective catalytic reduction of nitrogen oxides by ammonia and the oxidation of decane by oxygen.

The manufacture of geopolymer-based catalysts by utilization of solid wastes has many benefits such as low-cost, environment-friendly, energy-saving and resource-recycling. The steel slag is a by-product from the conversion of pig iron to steel and the methylene blue (MB) dye is one of the organic pollutants in waste water disposed by the dyeing and printing textiles. In order to realize the dual purposes of the resource recycling of steel slag and remove organic pollutants from the waste water, a new type of Ni,Ca-cementitious material is firstly synthesized by alkali-activated steel slag polymerization and ion exchange, and used as a catalyst for the photocatalytic degradation of MB under UV irradiation in this paper.

2. Experimental methods

2.1. Materials

The steel slag with a specific surface area of 450 $m^2\ kg^{-1}$ and an average particle size of 17.49 μm was obtained from Laiwu Steel Company after ball-milling 1 h. The main chemical components in weight percent are shown in Table 1. A chemical activator, NaOH (A.P.), was purchased from Xi'an Chemical Reagent Company.

2.2. Preparation of Na,Ca-cementitious material

The starting materials of steel slag and activator for respectively providing charge compensations of Ca^{2+} and Na^+ cations were mixed in the mass ratio of steel slag/activator/water = 1:0.11:0.28. A typical preparation procedure was described as below. The steel slag was placed into a net paste stirrer containing an aqueous solution of alkaline activator, and sufficiently mingled for 2 min. The

* Corresponding author. Tel.: +86 29 82202467; fax: +86 29 85535724.
E-mail address: yaojzhang@yahoo.com.cn (Y.J. Zhang).

0304-3894/$ – see front matter © 2012 Elsevier B.V. All rights reserved.
doi:10.1016/j.jhazmat.2012.01.001

Table 1
Chemical components of specimens (wt%).

(wt%)	Na_2O	K_2O	NiO	SiO_2	Al_2O_3	CaO	Fe_2O_3	TiO_2	MgO	V_2O_5	MnO	P_2O_5	Loss on ignition
Steel slag	0.15	0.12	0	19.13	4.87	37.42	18.77	1.62	5.55	0.98	3.63	0.65	7.11
Na,Ca-cem*	4.01	0.10	0	18.78	3.36	35.40	15.99	1.35	3.21	0.88	3.05	0.59	13.28
NH_4-cem*	0.09	0.05	0	23.08	3.84	33.38	17.92	1.57	3.71	1.00	3.42	0.66	11.28
Ni,Ca-cem*	0.06	0.04	6.95	22.47	3.73	28.09	17.62	1.56	3.61	1.02	3.38	0.62	10.85

Note: Na,Ca-cem* is the Na,Ca-cementitious material; NH_4-cem* is the NH_4,Ca-cementitious material; Ni,Ca-cem* is the Ni,Ca-cementitious material.

slurry was cast into a 31.5 mm × 31.5 mm × 50 mm triplicate steel mold and then put into a curing box at 20 °C with 99% relative humidity for 1 day. After being demolded, the specimen was continuously cured at room temperature for additional 27 days [28]. Subsequently, the specimen with a compressive strength of 26 MPa was crushed and dried at 60 °C for 3 h in a nitrogen atmosphere to obtain a Na,Ca-cementitious material specimen with particle size in the range of 120 ~ 425 μm.

2.3. Preparation of Ni,Ca-cementitious material

The Na,Ca-cementitious material specimen (10 g) was added to 100 mL aqueous solution of 0.3 M NH_4Ac at room temperature for 12 h to perform ion exchange of Na^+ with NH_4^+. The specimen was filtrated and washed sufficiently with deionized water and then dried at 60 °C for 3 h in a nitrogen atmosphere. As mentioned above, the experimental procedure was repeated once more to get the NH_4-cementitious material specimen.

The NH_4-cementitious material specimen (10 g) was added to 100 mL aqueous solution of 0.1 M $Ni(NO_3)_2$ to carry out ion exchange of NH_4^+ with Ni^{2+} at room temperature for 12 h. The specimen was filtrated and sufficiently washed with deionized water and then dried at 60 °C for 3 h in a nitrogen atmosphere to acquire a Ni,Ca-cementitious material-based catalyst. The chemical components are shown in Table 1.

2.4. Characterization of specimen

X-ray diffraction patterns of specimens were measured on a D/MAX-2400 X-ray diffractometer equipped with a rotation anode using CuKα irradiation. Diffuse reflectance UV–vis near infrared ray spectrum was recorded on a HITACHI UV-4100 spectrophotometer. Elemental analysis was carried out on a Bruker S4 Pioneer X-ray fluorescence (XRF) analyzer.

2.5. Photocatalytic reaction

The specimen (0.2 g) was added to 100 mL aqueous solution of MB dye (4.01×10^{-3} M) and placed in a 250 mL beaker. The solution was magnetically stirred and placed it in the dark for 30 min to establish an adsorption and desorption equilibrium. The aqueous solution of MB was then irradiated by a UV-lamp (ZW-2, 40 W) with a 254 nm output, and subsequently was centrifuged in each 20 min interval and the absorbance of the supernatant solution was monitored on a UV–vis spectrophotometer at the maximum absorption wavelength of 665 nm. The photocatalytic degradation rate was calculated by Eq. (1).

$$\eta = \left[\frac{A_{c0} - A_{ct}}{A_{c0}}\right] \times 100 \quad (1)$$

where η is the degradation ratio of MB. The A_{c0} and A_{ct} are the absorbency of MB solution at initial time and at time t after UV irradiation at 665 nm, respectively.

3. Results and discussion

3.1. Microstructure and absorption spectrum of specimen

Table 1 shows the chemical components of specimens. The content of Na_2O in steel slag powders is about 0.15 wt% and dramatically increases to 4.01 wt% in Na,Ca-cementitious material due to the polymerization of steel slag activated by sodium hydroxide. After Na^+ ions in turn are exchanged by NH^{4+} and Ni^{2+} ions, the amount of Na_2O rapidly drops to 0.06 wt% and the content of NiO is up to 6.95 wt%. This means almost all the Na^+ ions in the matrix of Na,Ca-cementitious material were replaced by Ni^{2+} ions at room temperature. Sazama et al. [27] reported that the Na^+ ions in the vicinity of all the Al atoms in the geopolymer network could be exchanged by Cu^{2+} or Co^{2+} ions at room temperature.

Fig. 1 shows the XRD patterns of specimens. The steel slag powders show some mineral phases, such as calcium iron oxide ($Ca_2Fe_2O_5$, JCPDS No. 19-0222), Belite (Ca_2SiO_4, JCPDS No. 98-000-0275), alite (Ca_3SiO_5, JCPDS No. 98-000-0043), portlandite ($Ca(OH)_2$, JCPDS No. 98-000-0359) and wustite (FeO, JCPDS No. 46-1312). The details about these mineral phases including chemical formula, serial number of JCPDS and 2θ are summarized in Table 2. The intensities of some diffraction peaks remarkably decrease and some peaks disappear in the pattern of Na,Ca-cementitious material compared with the pattern of steel slag powders in Fig. 1, suggesting that the mineral phases in the steel slag such as $Ca_2Fe_2O_5$, $Ca(OH)_2$, Ca_2SiO_4 and Ca_3SiO_5, partially react with aqueous alkaline solution of sodium hydroxide to produce two kinds of new hydrated products, metahalloysite ($Si_2Al_2O_5(OH)_2$, JCPDS No. 01-074-1023) and calcium silicate hydrate (CSH) ($Ca_{1.5}SiO_{3.5}{\cdot}xH_2O$, JCPDS No. 33-0306) [29]. Yip et al. [30] reported that it could be able to produce Na-geopolymer gel, Ca-geopolymer gel, and CSH gel in a metakaolin/GGBFS system. From Fig. 1 it can be observed that the pattern of Ni,Ca-cementitious material is similar to that of

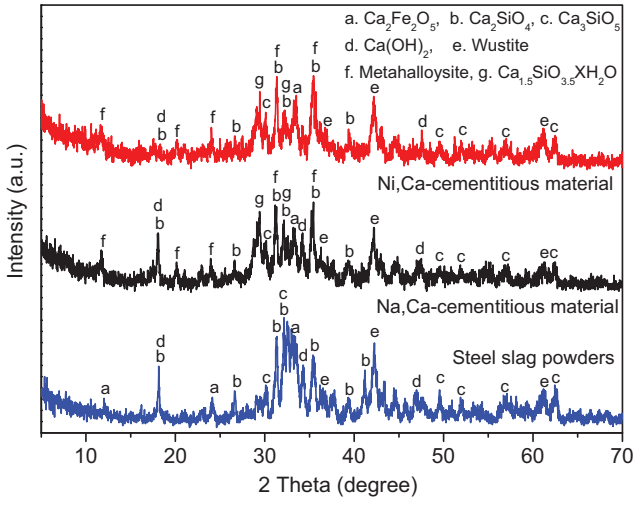

Fig. 1. X-ray diffraction patterns of specimens.

Table 2
Mineral phases of specimens.

Mineral phase	Chemical formula	Number of JCPDS	2θ (°)
Calcium iron oxide	$Ca_2Fe_2O_5$	19-0222	12.00, 24.11, 33.35
Belite	Ca_2SiO_4	98-000-0275	18.08, 26.50, 31.19, 32.09, 35.36, 39.52, 41.28, 56.61
Alite	Ca_3SiO_5	98-000-0043	30.12, 32.24, 49.54, 51.92, 56.61, 62.45
Portlandite	$Ca(OH)_2$	98-000-0359	18.08, 34.11, 47.10
Wustite	FeO	46-1312	36.34, 42.15, 61.13
Metahalloysite	$Si_2Al_2O_5(OH)_4$	01-074-1023	11.48, 20.12, 23.85, 31.27, 35.36
Calcium silicat hydrate	$Ca_{1.5}SiO_{3.5}\cdot xH_2O$	33-0306	29.32, 32.09

Na,Ca-cementitious material except for the diminution of peak intensities of portlandite.

Fig. 2 shows the diffuse reflectance UV–vis near infrared ray spectra of specimens. There are typical absorption bands in the range of 230 ~ 300 nm and they are much clearer after enlargement (the left top of Fig. 2). Absorption bands centered at 260.6 nm and 281.5 nm are observed in the Na,Ca-cementitious material specimen, while these bands are slightly blue-shifted to 257.3 nm and 271.1 nm respectively in the Ni,Ca-cementitious material. The blue-shifted bands are probably attributed to the strong interaction of Ni^{2+} and negative charge of $[AlO_4]^{5-}$ tetrahedron in the framework of cementitious material as a result of Ni^{2+} ion (0.069 nm) with smaller ionic radius than Na^+ ion (0.102 nm). In the near infrared ray region, three kinds of absorption bands centered at 1404 nm, 1922 nm and 2215 nm are suggested to be the absorption bands of Si—OH in the frameworks of Na,Ca-cementitious and Ni,Ca-cementitious materials. Elsherbiny et al. [31] reported that the porous silica powders show a shielded complex ≡SiO—H(OH_2) absorption band at 1404 nm.

3.2. Photocatalytic activities of specimens

Fig. 3 exhibits the photocatalytic degradation activities of specimens for MB. In order to understand comprehensively the different degradation activities, three approaches are taken in the catalytic reactions. The first way is that the aqueous solution of MB is exposed to UV light without catalyst. The second way is that the aqueous solution of MB suspending catalyst is put in the dark without UV irradiation. The third way is that the aqueous solution of MB containing catalyst is exposed to UV light. The degradation rate of 22.97% in the first way presents that the MB has the low photodegradation activity. The results in the second way show the degradation rate of 15.09% on the Na,Ca-cementitious materials and 29.25% on the Ni,Ca-cementitious materials. These low degradation activities can be dominantly ascribed to the catalytic degradation, suggesting that the MB molecules firstly absorb on the surface of catalyst, then are catalytically degraded and are finally desorbed from the catalyst. It can be observed from Fig. 3 in the third way that the Ni,Ca-cementitious materials-based catalyst shows the photocatalytic degradation rate of 94.39% and the Na,Ca-cementitious materials displays 53.27% under UV irradiation, respectively. By comparing, the order of the degradation rate of MB on the Ni,Ca-cementitious materials is the photocatalytic degradation (the catalyst irradiated by UV) ≫ the catalytic degradation (without UV) > the photodegradation (without catalyst). The highest photocatalytic degradation rate of MB on Ni,Ca-cementitious materials-based catalyst is considered to be the results of synergistic effect among the matrix of cementitious material, Ni^{2+} ions and the iron oxides of wustite (FeO) and calcium iron oxide ($Ca_2Fe_2O_5$) from the steel slag.

3.3. Reaction mechanism

A possible mechanism for photocatalytic oxidative degradation of MB is proposed as following. From Fig. 1 it is known that the iron species predominately exists in the forms of wustite (FeO) and calcium iron oxide ($Ca_2Fe_2O_5$) dispersed in the network of Ni,Ca-cementitious materials. These iron oxides, FeO and $Ca_2Fe_2O_5$, show semiconductor properties with narrow band gaps. When the energy of a photon is absorbed by an electron situated in valence band of iron oxides under UV light irradiation, the photogenerated electron (e^-) from the valence band jumps to its conduction band and simultaneously leaves behind a positive hole (h^+) in the valence band as shown in Eq. (2) and Fig. 4. Gulshan et al. [32] reported that the iron oxides of maghemite and hematite show semiconductor properties and have the activities of photodecomposition of MB by illuminating with UV, visible and solar radiation. Yang et al. [33] reported that the $Ca_2Fe_2O_5$ was employed as a catalyst for photodegradation of methyl orange under UV light irradiation.

$$\text{Iron oxides} \xrightarrow{hv} e^- + h^+ \quad (2)$$

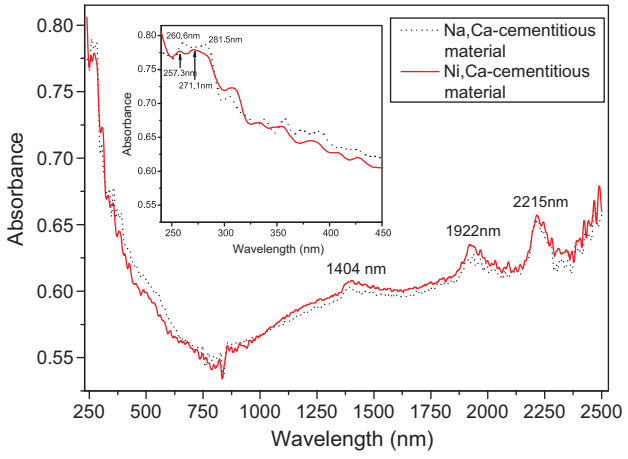

Fig. 2. Diffuse reflectance UV–vis near infrared ray spectra of specimens.

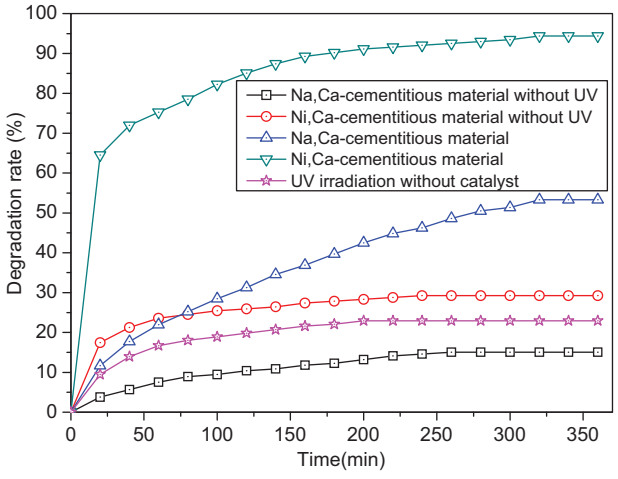

Fig. 3. Photocatalytic degradation rate of MB under UV light irradiation.

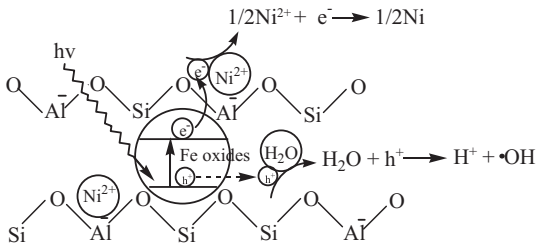

Fig. 4. Schematic representation of reaction mechanism.

The photogenerated electron (e^-) transfers to Ni^{2+} ions located in the vicinity of $[AlO_4]^{5-}$ tetrahedron with negative charge in the framework of cementitious materials as shown in Eq. (3) and Fig. 4. Therefore, the Ni^{2+} ions play important roles in the transmission photogenerated electron and the enhancement of separation efficiency of photogenerated electron–hole pairs.

$$(1/2)Ni^{2+} + e^- \rightarrow (1/2)Ni \quad (3)$$

The photogenerated hole (h^+) reacts with H_2O molecule to release a significant proportion of hydroxyl radicals which is the primary oxidant in the photocatalytic oxidation of organic compounds depicted in Eq. (4) and Fig. 4 [34,35].

$$H_2O + h^+ \rightarrow H^+ + {\bullet}OH \quad (4)$$

The electrode potential of hydroxyl radical (2.8 V) is much higher than that of MB (0.53 V) in aqueous solution so that the MB can be photocatalytically oxidized by hydroxyl radical via demethylation, cleavage of chromophore ring and final degradation into CO_2, H_2O, NO_3^- and SO_4^{2-} exhibited in Eq. (5) [36,37].

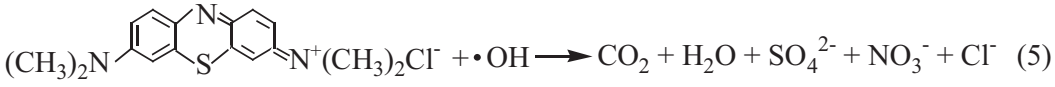

(5)

4. Conclusion

A novel Ni,Ca-cementitious materials-based catalyst was prepared via a two-step reaction of polymerization and ion exchange. There are two kinds of hydrated products, metahalloysite ($Si_2Al_2O_5(OH)_4$) and calcium silicate hydrate (CSH) in the alkali-activated steel slag-based cementitious materials. The blue-shift of absorption bands in the UV region was suggested to be the strong interaction of Ni^{2+} and the negative charge of $[AlO_4]^{5-}$ tetrahedron, while the absorption bands in near infrared region were suggested to be the absorption of silicon-hydroxyl (Si—OH) in the framework of Ni,Ca-cementitious materials. In the process of photocatalytic oxidative degradation of MB, the Ni^{2+} ions act as a critical role in transmission of photogenerated electrons and the iron oxides are responsible for the transfer of photogenerated holes so as to enhance separation efficiency of the electron–hole pairs and improve the photocatalytic efficiency.

Acknowledgements

This work was financially supported by Industrial Key Project of Shaanxi Province (No. 2010K01-080), and Open Fund of State Key Laboratory of Architecture Science and Technology in West China (XAUAT), Xi'an University of Architecture and Technology (No. 10KF05).

References

[1] F. Pacheco-Torga, J. Castro-Gomes, S. Jalali, Alkali-activated binders: a review. Part 1. Historical background, terminology, reaction mechanisms and hydration products, Constr. Build. Mater. 22 (2008) 1305–1314.
[2] J.S.J. van Deventer, J.L. Provis, P. Duxson, G.C. Lukey, Reaction mechanisms in the geopolymeric conversion of inorganic waste to useful products, J. Hazard. Mater. 139 (2007) 506–513.
[3] J. Temuujin, A. van Riessen, K.J.D. MacKenzie, Preparation and characterization of fly ash based geopolymer mortars, Constr. Build. Mater. 24 (2010) 1906–1910.
[4] I.G. Richardson, J.G. Cabrera, The nature of C—S—H in model slag-cements, Cem. Concr. Compos. 22 (2000) 259–266.
[5] I.G. Richardson, C.R. Wilding, M.J. Dickson, The hydration of blast-furnace slag cements, Adv. Cem. Res. 2 (1989) 147–157.
[6] Y.J. Zhang, Y.L. Zhao, H.H. Li, D.L. Xu, Structure characterization of hydration products generated by alkaline activation of granulated blast furnace slag, J. Mater. Sci. 43 (2008) 7141–7147.
[7] D. Khate, R. Chaudhary, Mechanism of geopolymerization and factors influencing its development: a review, J. Mater. Sci. 42 (2007) 729–746.
[8] E. Belhadj, C. Diliberto, A. Lecomte, Characterization and activation of basic oxygen furnace slag, Cem. Concr. Compos. 34 (2012) 34–40.
[9] D. Lonescu, T.R. Meadowcroft, P.V. Barr, Early-age hydration kinetics of steel slag, Adv. Cem. Res. 13 (2001) 21–30.
[10] S. Hu, H. Wang, G. Zhang, Q. Ding, Bonding and abrasion resistance of geopolymeric repair material made with steel slag, Cem. Concr. Compos. 30 (2008) 239–244.
[11] F. Pacheco-Torgal, J. Castro-Gomes, S. Jalali, Alkali-activated binders: a review. Part 2. About materials and binders manufacture, Constr. Build. Mater. 22 (2008) 1315–1322.
[12] P. Duxson, A. Fernandez-Jimenez, J.L. Provis, G.C. Lukey, A. Palomo, J.S.J. van Deventer, Geopolymer technology: the current state of the art, J. Mater. Sci. 42 (2007) 2917–2933.
[13] S. Songpiriyakij, T. Pulngern, P. Pungpremtrakul, C. Jaturapitakkul, Anchorage of steel bars in concrete by geopolymer paste, Mater. Des. 32 (2011) 3021–3028.
[14] G. Habert, J.B. d'Espinose de Lacaillerie, N. Roussel, An environmental evaluation of geopolymer based concrete production: reviewing current research trends, J. Clean. Prod. 19 (2011) 1229–1238.
[15] M.Y. Khalil, E. Merz, Immobilization of intermediate-level wastes in geopolymers, J. Nucl. Mater. 211 (1994) 141–148.
[16] J.G.S. van Jaarsveld, J.S.J. van Deventer, L. Lorenzeni, The potential use of geopolymeric materials to immobilize toxic metals: part I. Theory and applications, Miner. Eng. 10 (1997) 659–669.
[17] Y.L. Galiano, C. Fernandez Pereira, J. Vale, Stabilization/solidification of a municipal solid waste incineration residue using fly ash-based geopolymers, J. Hazard. Mater. 185 (2011) 373–381.
[18] D.L.Y. Kong, J.G. Sanjayan, Effect of elevated temperatures on geopolymer paste, mortar and concrete, Cem. Concr. Res. 40 (2010) 334–339.
[19] J. Temuujin, W. Rickard, M. Lee, A. van Riessen, Preparation and thermal properties of fire resistant metakaolin-based geopolymer-type coatings, J. Non-Cryst. Solids 357 (2011) 1399–1404.
[20] Y. Huang, M. Han, The influence of α-Al_2O_3 addition on microstructure, mechanical and formaldehyde adsorption properties of fly ash-based geopolymer products, J. Hazard. Mater. 193 (2011) 90–94.
[21] K. Al-Zboona, M.S. Al-Harahsheh, F.B. Hani, Fly ash-based geopolymer for Pb removal from aqueous solution, J. Hazard. Mater. 188 (2011) 414–421.
[22] L. Li, S. Wang, Z. Zhu, Geopolymeric adsorbents from fly ash for dye removal from aqueous solution, J. Colloid Interface Sci. 300 (2006) 52–59.
[23] J. Davidovits, Geopolymers: inorganic polymeric new materials, J. Therm. Anal. 37 (1991) 1633–1656.
[24] K. Komnitsas, D. Zaharaki, Geopolymerisation: a review and prospects for the minerals industry, Miner. Eng. 20 (2007) 1261–1277.
[25] O. Bortnovsky, J. Dedecek, Z. Tvaruzkova, Z. Sobalik, J. Subrt, Metal ions as probes for characterization of geopolymer materials, J. Am. Ceram. Soc. 91 (2008) 3052–3057.
[26] S.J. O'Connor, K.J.D. MacKenzie, M.E. Smith, J.V. Hanna, Ion exchange in the charge-balancing sites of aluminosilicate inorganic polymers, J. Mater. Chem. 20 (2010) 10234–10240.
[27] P. Sazama, O. Bortnovsky, J. Dedecek, Z. Tvaruzkova, Z. Sobalík, Geopolymer based catalysts—new group of catalytic materials, Catal. Today 164 (2011) 92–99.
[28] Y.J. Zhang, Y.C. Wang, D.L. Xu, S. Li, Mechanical performance and hydration mechanism of geopolymer composite reinforced by resin, Mater. Sci. Eng. A 527 (2010) 6574–6580.
[29] K. Sagoe-Crentsil, L. Weng, Dissolution processes, hydrolysis and condensation reactions during geopolymer synthesis. Part II. High Si/Al ratio systems, J. Mater. Sci. 42 (2007) 3007–3014.

[30] C.K. Yip, G.C. Lukey, J.S.J. Van Deventer, The coexistence of geopolymeric gel and calcium silicate hydrate at the early stage of alkaline activation, Cem. Concr. Res. 35 (2005) 1688–1697.
[31] A.S. Elsherbiny, H.J. Egelhaaf, D. Oelkrug, Accessibility and shielding of silanol surface centers on porous silica beads; UV/vis absorption and fluorescence studies, J. Photochem. Photobiol. A 220 (2011) 39–46.
[32] F. Gulshan, S. Yanagida, Y. Kameshima, T. Isobe, A. Nakajima, K. Okada, Various factors affecting photodecomposition of methylene blue by iron-oxides in an oxalate solution, Water Res. 44 (2010) 2876–2884.
[33] Y. Yang, Z. Cao, Y. Jiang, L. Liu, Y. Sun, Photoinduced structural transformation of $SrFeO_3$ and $Ca_2Fe_2O_5$ during photodegradation of methyl orange, Mater. Sci. Eng. B 132 (2006) 311–314.
[34] M.A. Valenzuela, P. Bosch, J. Jimenez-Becerrill, O. Quiroz, A.I. Paez, Preparation, characterization and photocatalytic activity of ZnO, Fe_2O_3 and $ZnFe_2O_4$, J. Photochem. Photobiol. A 148 (2002) 177–182.
[35] L. Zhang, X. Zhou, X. Guo, X. Song, X. Liu, Investigation on the degradation of acid fuchsin induced oxidation by $MgFe_2O_4$ under microwave irradiation, J. Mol. Catal. A: Chem. 335 (2011) 31–37.
[36] T. Zhang, T. Oyama, A. Aoshima, H. Hidaka, J. Zhao, N. Serpone, Photooxidative *N*-demethylation of methylene blue in aqueous TiO_2 dispersions under UV irradiation, J. Photochem. Photobiol. A 140 (2001) 163–172.
[37] A. Houas, H. Lachheb, M. Ksibi, E. Elaloui, C. Guillard, J. Herrmann, Photocatalytic degradation pathway of methylene blue in water, Appl. Catal. B 31 (2001) 145–157.